



## Relaxation time effects of wave ripples on tidal beaches

M. J. Austin,<sup>1</sup> G. Masselink,<sup>2</sup> T. J. O'Hare,<sup>1</sup> and P. E. Russell<sup>1</sup>

Received 15 May 2007; revised 9 July 2007; accepted 23 July 2007; published 24 August 2007.

[1] Seabed roughness due to wave ripples is a key factor in controlling sediment transport processes in the nearshore zone. Roughness is commonly considered a function of the ripple geometry, which in turn, can be predicted from sediment and hydrodynamic parameters. Existing ripple predictors consider the bed morphology to be in equilibrium with the hydrodynamics, whereas recent laboratory measurements show that the time scale for ripple development is of the order of tens of minutes to hours. Here we show that wave ripples on tidal beaches are significantly affected by relaxation time effects, with ripple height and length progressively increasing during the rising tide and remaining constant during the falling tide. Moreover, we examine the ripples in the context of existing empirical models and suggest how the temporal evolution over a tidal cycle may be predicted. **Citation:** Austin, M. J., G. Masselink, T. J. O'Hare, and P. E. Russell (2007), Relaxation time effects of wave ripples on tidal beaches, *Geophys. Res. Lett.*, *34*, L16606, doi:10.1029/2007GL030696.

### 1. Introduction

[2] Bedform ripples are ubiquitous features in the nearshore of sandy beaches and are of fundamental importance to sediment transport processes [Fredsoe and Deigaard, 1992]. Firstly, ripples represent roughness elements, which to a large degree determine the structure of the bottom boundary layer [Grant and Madsen, 1986]. Secondly, through the generation of near-bed turbulence, ripples significantly affect the vertical profile of suspended sediment, and the magnitude and direction of suspended sediment fluxes [Vincent *et al.*, 1991]. It is not surprising, therefore, that considerable effort has been expended on predicting ripple occurrence and geometry from hydrodynamic and sediment parameters [e.g., Wiberg and Harris 1994].

[3] Ripples are a response to the transport of sediment within the boundary layer, which grow and steepen until at some critical geometry an energetic lee vortex is formed [Tunstall and Inman, 1975]. In response to greater orbital amplitudes, the vortex scours sediment from the ripple trough regions to the crest increasing ripple size. After some finite time, when ripple geometry is in equilibrium with the hydrodynamic forcing, the ripples attain an approximately constant steepness of  $\sim 0.17$  [Nielsen, 1981]. As forcing increases, ripple crests undergo erosion until sheet flow flattens the bed.

[4] Recent debate has focused on whether ripples are in equilibrium with the hydrodynamics or if they are influenced by relaxation time effects [Smith and Sleath, 2005; Soulsby and Whitehouse, 2005; Doucette and O'Donoghue, 2006]. In other words, do ripples have a reaction time whereby the interval between the hydrodynamic disturbance and the resultant morphological change is almost instantaneous, or is the adjustment period sufficiently long that the morphological change significantly lags the changes in forcing. Various ripple predictors [e.g., Wiberg and Harris, 1994; Williams *et al.*, 2004] relate the bedform geometry to bed shear stress, so assume that ripple geometry is intrinsically coupled to the forcing. However, others argue that once ripples are established, relaxation effects mean that it is difficult to change the wavelength [Marsh *et al.*, 1999]. A further complicating factor in the field may be the presence of relic ripple populations, which are a legacy of previous higher energy conditions [Traykovski *et al.*, 1999], and out of equilibrium with the flow.

[5] The objectives of this paper are to use field data collected from a mesotidal sandy beach subjected to variable wave conditions to investigate the occurrence of ripple relaxation effects. To date, no measurements of ripple relaxation time effects have been reported from tidal beaches, and it is demonstrated that these effects are highly significant throughout the falling stage of the tide.

### 2. Methodology

[6] During a 3-week field campaign in May 2006 at Truc Vert beach, SW France, morphological, hydrodynamic and sedimentological data were collected over 15 tidal cycles spanning a range of wave ( $H_s = 1-2$  m) and tide conditions (range = 1.3–3.3 m). Ripples were an enduring feature of the intertidal beachface and were monitored along 2 m shore normal profiles using acoustic Sand Ripple Profilers mounted 0.7 m above the bed on the crest and landwards trough of an intertidal bar (SRP, Figure 1). The SRP acoustic returns were converted to ripple dimensions by applying standard time series analysis techniques to the spatial bed level data. Ripple length  $\lambda$  was determined as twice the spatial lag corresponding to the strongest negative auto-correlation peak and ripple height  $\eta$  as the root mean square wave height equivalent using  $\sqrt{8}\sigma$ , where  $\sigma$  is the standard deviation of the bed level profile. Data were subsequently processed following Masselink *et al.* [2007] and combined to produce 10-min averages. The bed shear stress was quantified by the Shields parameter

$$\theta = \frac{0.5f_w U_m^2}{(s-1)gD}, \quad (1)$$

where  $U_m$  is the wave orbital velocity ( $=\sqrt{8}\sigma_u$ , where  $\sigma_u$  is the standard deviation of the cross-shore velocity),  $s$  is the

<sup>1</sup>School of Earth, Ocean and Environmental Sciences, University of Plymouth, Plymouth, UK.

<sup>2</sup>School of Geography, University of Plymouth, Plymouth, UK.

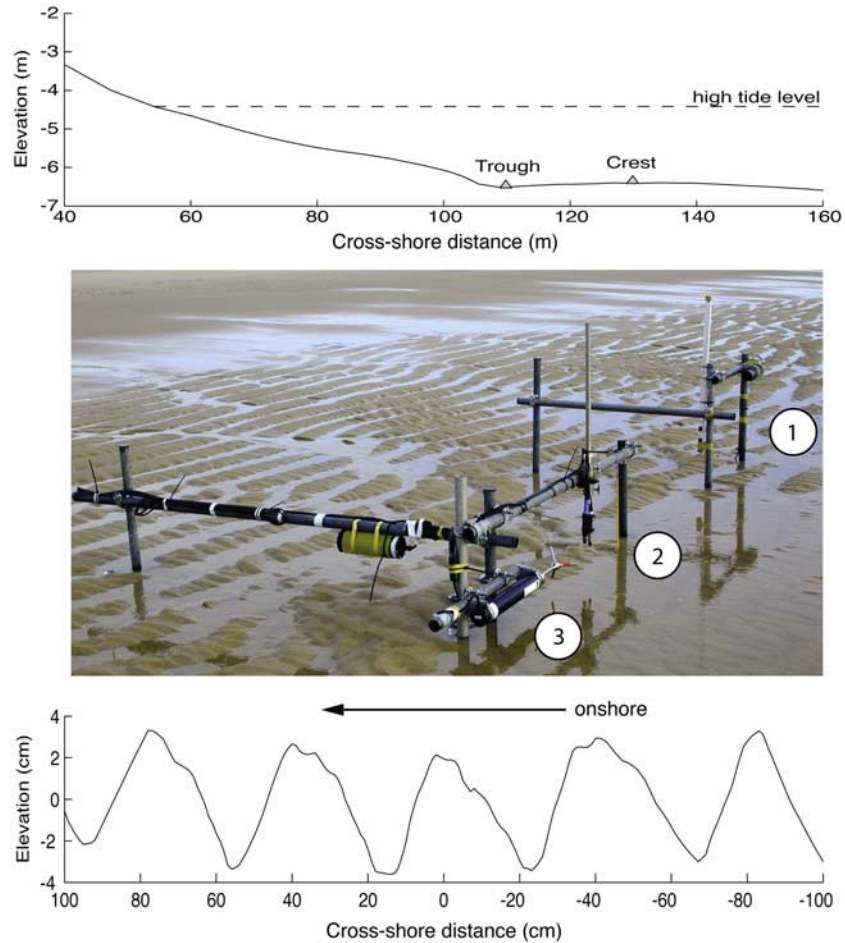


**Figure 1.** Illustration of the field setting. (top) Beach profile indicating position of SRPs. (middle) Rippled bed exposed at low tide indicating the instruments: (1) sand ripple profiling sonar, (2) optical backscatter sensor, and (3) Acoustic Doppler current meter. (bottom) Single cross-shore ripple swath recorded by the SRP.

specific gravity of sand,  $D$  is the median grain diameter and  $g$  is gravity. The wave friction factor  $f_w$  is defined as [Swart, 1974]

$$f_w = \exp\left[5.213(k_s/A)^{0.194} - 5.977\right], \quad (2)$$

where  $k_s$  is the Nikuradse roughness length ( $= 2.5D$ ), and  $A$  the orbital amplitude ( $= U_m T/\pi$ , where  $T$  is the significant wave period). This resulted in 732 coincident data segments of ripple geometry and hydrodynamics. Sediment samples were analyzed using sieving and settling tube methods to yield sediment size and fall velocity ( $D = 0.49$  mm;  $w_s = 0.064$  m s<sup>-1</sup>).

### 3. Temporal Bedform Evolution

[7] Figure 2 shows a typical time series of bed evolution. There are three key points to observe: (1) initially, small ripples ( $\lambda = 20$  cm,  $\eta = 3.5$  cm) migrate rapidly onshore; (2) after 1.5 hrs,  $\eta$  and  $\lambda$  double; (3) the large ripples remain stable throughout the ebb tide. The coincident hydrodynamics are very different.  $U_m$  and  $\theta$  are symmetrically distributed, with similar values at comparable stages of the flood and ebb tide, caused by the relative movement of the SRPs

from the inner to the outer surf zone as the tide modulates the spatial distribution of wave breaking. The vector mean current velocity is  $O(10^{-2})$  m s<sup>-1</sup>, an order of magnitude less than  $U_m$  and consistent with below threshold of motion values of the Shields parameter ( $\theta < 0.05$ ); this suggests that waves, rather than currents, force ripple evolution.

[8] Ripple evolution during the rising and falling phases of the tide are clearly different and cannot be in equilibrium during both. Figure 3 presents ensemble averages for all the data collected during the field experiment, normalized with respect to high tide. The forcing parameters typically used for ripple prediction,  $\theta$  and  $d_0$  ( $= 2A$ ), are symmetrically distributed around the high tide at both cross-shore locations. Conversely, the morphological response of the ripples is asymmetric, with  $\eta$  and  $\lambda$  increasing during the flood and remaining stable during the ebb tide.

[9] It is informative to quantify the ripples in terms of existing classification schemes and the hydrodynamic parameters frequently used in equilibrium ripple predictors. Figure 4a plots  $\lambda$  versus  $d_0$  from both cross-shore locations, non-dimensionalised by  $D$ , and indicates the *Wiberg and Harris* [1994] model, hereinafter referred to as WH. The present ripples are steep ( $\eta/\lambda \geq 0.15$ ) *vortex* ripples [Bagnold, 1963], which plot about the WH division

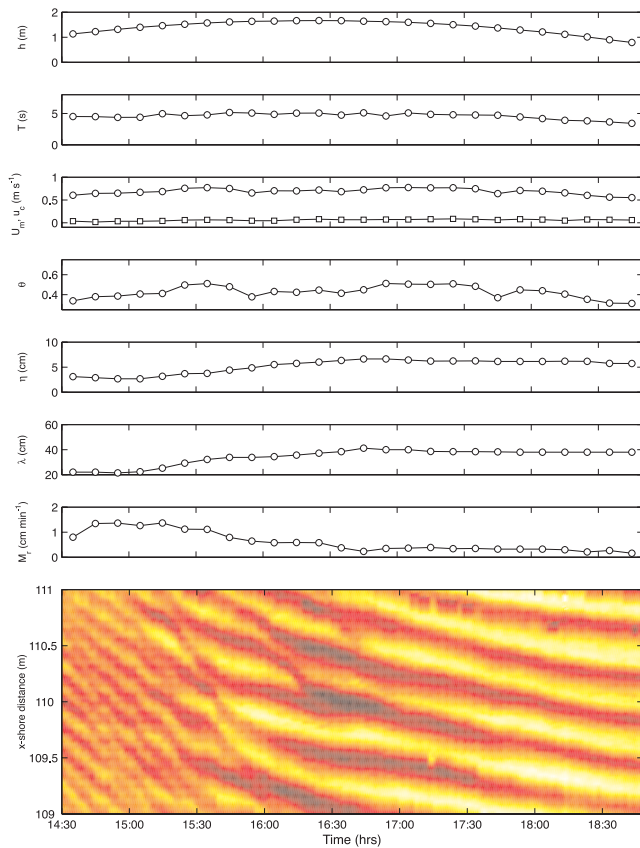


**Figure 2.** Hydrodynamic and ripple evolution during a tidal cycle: (top to bottom) water level  $h$ , wave period  $T$ , maximum orbital velocity  $U_m$  ( $\circ$ ) and vector mean current velocity  $u_c$  ( $= \sqrt{u^2 + v^2}$ , square), Shields parameter  $\theta$ , ripple height  $\eta$ , ripple length  $\lambda$ , ripple migration rate  $M_r$ , and surface plot of ripple evolution. Coloring indicates elevation between  $-6.5$  cm (black) and  $+5$  cm (white).

between the *suborbital* regime, for which  $\lambda$  depends on both  $d_0$  and  $D$ , and the *anorbital* regime where  $\lambda$  depends only on  $D$ ; these have been termed *short wave ripples* by Williams *et al.* [2005]. The positive trend between  $\lambda/D$  and  $d_0/D$  during the flood tide is similar to that observed by Becker *et al.* [2007], suggesting that the effects of suspended sediment are important and hence the ripples are not *suspension-limited* [Smith and Wiberg, 2006]. The linear relationship between the flood tide  $\lambda$  and  $d_0$  indicates that  $\lambda$  is actively forced by waves, but the slope of the present data ( $0.048d_0$ ) is less than that reported by Traykovski *et al.* [1999],  $0.75d_0$  but similar to Becker *et al.* [2007],  $0.09d_0$ . Further insight is gained by plotting the ripples in the context of the recent suborbital model of Williams *et al.* [2004], where it is clear that for a given bed stress, the model over-predicts  $\lambda$  in a similar manner to the WH model or a traditional orbital scaling (Figure 4b).

[10] The flood tide ripples respond to wave forcing, but are not well scaled by existing models. For the present case, it is practical to plot the ripples as a function of bottom stress in  $[\theta, \lambda]$  space (Figure 4c). Flood tide  $\lambda$  increases with  $\theta$  and is well described by the equilibrium relation  $\lambda = 0.49\theta$ . However, during the ebb tide,  $\lambda$  plots above and to the left of the equilibrium line and is thus independent of  $\theta$ ;

either  $\lambda$  is too large, or  $\theta$  too small, and hence there is no discernible change in  $\lambda$  during the ebb. Figures 4d–4e plot the ripple trajectory in  $[\theta, \lambda]$  and  $[\theta, \eta]$  space during four individual tides and demonstrate the tide-induced hysteresis that is typical for all tides. Clearly, the ripples must adjust at some point, because the dimensions at the beginning of the flood are consistent from tide-to-tide. Visual observations suggested that it was the action of swash, at the tail of the ebb and beginning of the flood, that acted to ‘reset’ the ripple geometry and complete the hysteresis loop by flattening the ripple crests and reducing their steepness.

#### 4. Discussion and Conclusions

[11] Field data demonstrate that wave ripples are strongly influenced by relaxation time effects, taking a finite amount of time to respond to changing hydrodynamic conditions. Recent laboratory measurements indicate that the time scale for ripple development may be of the order of hours and depends on the flow rather than the initial bed configuration. Following Doucette and O’Donoghue [2006, equation (4)], the theoretical time-to-equilibrium for the flood tide adjustment period, computed using the measured flow, is 5–10 min. This is in good agreement with the observations and suggests that the flood tide ripples are near equilibrium and adjust to the increased forcing, however, existing equilibrium models [e.g., Wiberg and Harris, 1994; Williams *et al.*, 2004] perform badly. The reasons for the breakdown of the existing models during the flood tide are unclear. Given that the ripples scale with forcing and have a 5–10 min relaxation time, this strongly suggests that they are close to equilibrium and should therefore be reasonably predicted. The surf zone origin of the present data probably provides the best indication for the failure of the models, since the increased non-linearity and near-breaking wave conditions are very different to those of the shoaling wave and continental shelf regions from where the models have primarily been formulated. This equilibrium relationship subsequently breaks down, and the intriguing question is therefore: why do the ripples not respond to the reversal in flow conditions during the falling tide and evolve from large to smaller ripples?

[12] Despite practically identical trends in hydrodynamic forcing,  $\lambda$  and  $\eta$  progressively increase during the rising tide and remain constant during the falling tide. At the beginning of the flood, the small ripples are predominantly suborbital and as conditions become more energetic the ripples grow—by high tide the surf zone is populated with substantial anorbital ripples. During the falling tide, relaxation time causes hysteresis whereby, even in the energetic conditions ( $h < 2$  m;  $\theta = 0.5$ – $1.5$ ), changes in ripple geometry lag behind changes in hydrodynamic forcing. It seems likely that the ripples become too large to be changed by the waning energy conditions and hence become decoupled from the forcing and display arrested development. In other words, the tide modulates the hydrodynamic conditions at a rate that is far more rapid than the relaxation time of the large ebb ripples, and suggests that the initial bed configuration is critical to the observed response. This is supported by field observations made in relatively deep water ( $>4$  m) after storms that strongly suggest that it takes a

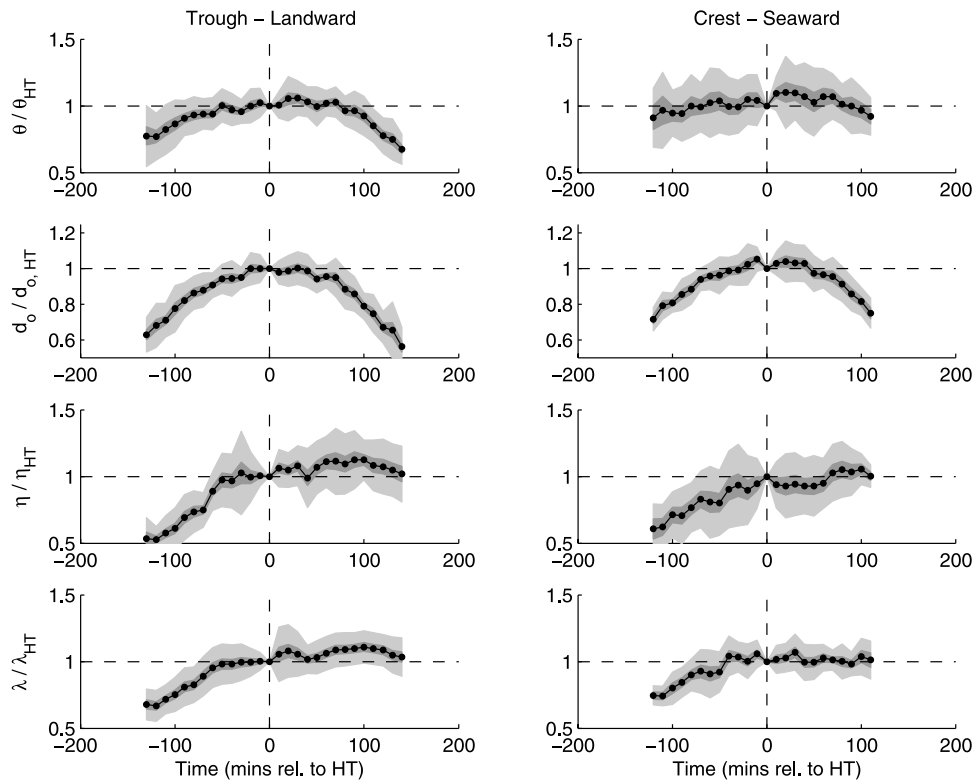


**Figure 3.** Shields parameter  $\theta$ , orbital diameter  $d_o$ , ripple height  $\eta$  and ripple length  $\lambda$  normalized with respect to high tide. Time is class-averaged and re-scaled relative to high tide and the vertical axis is normalized by the high tide value. Solid markers are the mean; light shading is the standard deviation  $\sigma$ , and dark shading the standard error  $\sigma/\sqrt{n}$  (where  $n$  is the number of observations in each class).

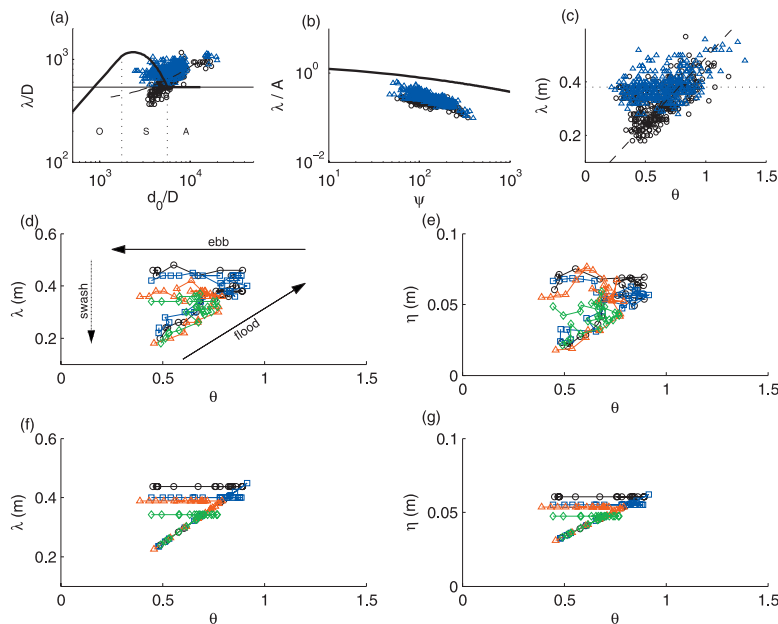


**Figure 4.** (a) Non-dimensional flood ( $\circ$ ) and ebb ( $\Delta$ ) ripple length showing the WH model (thick line): O, orbital; S, suborbital; A, anorbital) and with the anorbital scaling of  $\lambda = 535D$  continued beyond the transition region (thin line). The dashed curved line is the best fit to the flood tide data,  $0.048d_o + 0.18$ . (b) Ripple length normalized by  $A$  versus Mobility number  $\psi (= U_m^2/(s - 1)gD)$  indicating the *Williams et al.* [2004] model. (c) Ripple length plotted in  $[\theta, \lambda]$  space where the dashed line is the best-fit linear (equilibrium) model of  $\lambda = 0.49\theta$  ( $r^2 = 0.3$ ) and the horizontal dotted line the non-equilibrium trajectory. (d–e) Example ripple length and height trajectories demonstrating the tidal variation in  $[\theta, \lambda]$  and  $[\theta, \eta]$  and highlighting the hysteresis loop. (f–g) Predicted ripple length and height ( $r^2 = 0.79$  and  $0.76$ , respectively).

significant amount of time for established ripples to respond to a change of flow conditions [Traykovski et al., 1999].

[13] Relaxation time in bedform development may have significant implications for suspended sediment transport processes on tidal beaches. If the ripples are near-equilibrium during the rising tide but are over-developed during the falling tide due to relaxation effects, the larger ebb tide bed roughness causes enhanced sediment suspension, resulting in a tidal asymmetry in suspended sediment concentrations and fluxes. Davidson et al. [1993] and Masselink and Pattiaratchi [2000] both observed this phenomena, but the absence of convincing observations of the bed morphology precluded attributing the observed tidal asymmetry in sediment suspension to ripple hysteresis.

[14] To address the temporal development of the bed when relaxation effects are present in a tidal environment, the manner in which ripple predictors are applied must be reconsidered. Equilibrium predictors may perform adequately during the flood tide, but will fail during the ebb tide when flow and form are de-coupled and the ripples are moribund. Several laboratory-based formulations [Davis et al., 2004; Smith and Sleath, 2005; Doucette and O'Donoghue, 2006] use the exponential decay of the Logistic Growth Rule (LGR) to predict ripple evolution in response to a stepped change in flow. However, these are difficult to apply to field data since their extrapolated behavior to high shear stresses is unrealistic, and for the present case, the decay rate of the existing LGR models still depend on the flow and predict a 5–10 min ebb tide relaxation time as opposed to the observed time which is  $O(\text{hours})$ . Two recent field-based models, to some degree, capture the present observations. The Soulsby and Whitehouse [2005] model freezes ripples during a decrease in forcing, only allowing re-adjustment once conditions again become sufficiently intense (similar to the present case, where swash processes are required to adjust the substantial ebb ripples) or when bio-degradation is significant. The model of Traykovski [2007] also permits long wavelength ripples to persist after a wave event, and allows a reduction in ripple length by superimposing smaller ripples upon the existing morphology; however, the decay time-scale of both models is  $O(\text{days})$  and they are most suited to when the model input is a long time series of hydrodynamic conditions.

[15] The obvious solution to predicting ripple evolution for the present data utilizes their arrested ebb tide state. Throughout the rising tide the ripples are near equilibrium and may be modeled with an equilibrium-type predictor. It is then fairly simple to include a tide-based 'over-ride' into the model, whereby at high tide ripple evolution is stopped and the maximum size is maintained throughout the ebb. The best-fit linear model based on the flood tide ripple data is used to predict flood tide  $\lambda$  and  $\eta$  and an 'over-ride' is invoked at high tide, quantified by the maximum  $d_0$ , after which  $\lambda$  and  $\eta$  are conserved (Figures 4f–4g).

[16] The pragmatic and simple modelling approach proposed here provides a good overall description of the measured  $\eta$  and  $\lambda$  ( $r^2 = 0.76$  and  $0.79$ , respectively), but without the inclusion of data from other field sites, which is currently unavailable, remains limited in application. The approach is also only likely to work successfully in inter-

tidal settings, where tidally-driven changes in hydrodynamic conditions occur on much shorter time scales than those occurring in the subtidal zone due to storm activity.

[17] **Acknowledgments.** Peter Ganderton, Tony Butt, Jon Tinker, Tim Scott, Nadia Sénéchal, Tim Poate and Emma Rendle provided field assistance. This research was funded by NERC grant NER/A/S/2003/00553.

## References

- Bagnold, R. A. (1963), Beach and nearshore processes, in *The Sea*, edited by M. N. Hill, pp. 507–553, Wiley-Interscience, New York.
- Becker, J. M., Y. L. Firing, J. Aucan, R. Holman, M. Merrifield, and G. Pawlak (2007), Video-based observations of nearshore sand ripples and ripple migration, *J. Geophys. Res.*, *112*, C01007, doi:10.1029/2005JC003451.
- Davidson, M. A., P. E. Russell, D. A. Huntley, and J. Hardisty (1993), Tidal asymmetry in suspended sand transport on a macrotidal intermediate beach, *Mar. Geol.*, *110*, 333–353.
- Davis, J. P., D. J. Walker, M. Townsend, and I. R. Young (2004), Wave-formed sediment ripples: Transient analysis of ripple spectral development, *J. Geophys. Res.*, *109*, C07020, doi:10.1029/2004JC002307.
- Doucette, J. S., and T. O'Donoghue (2006), Response of sand ripples to change in oscillatory flow, *Sedimentology*, *53*, 581–596.
- Fredsoe, J., and R. Deigaard (1992), *Mechanics of Coastal Sediment Transport*, World Sci., Hackensack, N. J.
- Grant, W. D., and O. S. Madsen (1986), The continental-shelf bottom boundary-layer, *Annu. Rev. Fluid Mech.*, *18*, 265–305.
- Marsh, S. W., C. E. Vincent, and P. D. Osborne (1999), Bedforms in a laboratory flume: An evaluation of predictive models for bedform wavelength, *J. Coastal Res.*, *15*(3), 624–634.
- Masselink, G., and C. Pattiaratchi (2000), Tidal asymmetry in sediment resuspension on a macrotidal beach in northwestern Australia, *Mar. Geol.*, *163*, 257–274.
- Masselink, G., M. J. Austin, T. J. O'Hare, and P. E. Russell (2007), Geometry and dynamics of wave ripples in the nearshore zone of a coarse sandy beach, *J. Geophys. Res.*, doi:10.1029/2006JC003839, in press.
- Nielsen, P. (1981), Dynamics and geometry of wave-generated ripples, *J. Geophys. Res.*, *86*, 6467–6472.
- Smith, D., and J. F. A. Sleath (2005), Transient ripples in oscillatory flows, *Cont. Shelf Res.*, *25*, 485–501.
- Smith, J. J., and P. L. Wiberg (2006), Ripple geometry in wave-dominated environments, revisited, *Eos Trans. AGU*, *87*(36), Ocean Sci. Meet. Suppl., Abstract OS35D-24.
- Soulsby, R. L., and R. J. S. Whitehouse (2005), Prediction of ripple properties in shelf seas, *Final Tech. Rep. TR154(2)*, HR Wallingford, Wallingford, U. K.
- Swart, D. H. (1974), Offshore sediment transport and equilibrium beach profiles, *Lab. Publ. 131*, Delft Hydraul., Delft, Netherlands.
- Traykovski, P. (2007), Observations of wave orbital scale ripples and a nonequilibrium time-dependent model, *J. Geophys. Res.*, *112*, C06026, doi:10.1029/2006JC003811.
- Traykovski, P., A. E. Hay, J. D. Irish, and J. F. Lynch (1999), Geometry, migration, and evolution of wave orbital ripples at LEO-15, *J. Geophys. Res.*, *104*, 1505–1524.
- Tunstall, E. B., and D. L. Inman (1975), Vortex generation by oscillatory flow over rippled surfaces, *J. Geophys. Res.*, *80*, 3475–3484.
- Vincent, C. E., D. M. Hanes, and A. J. Bowen (1991), Acoustic measurements of suspended sand on the shoreface and the control of concentration by bed roughness, *Mar. Geol.*, *96*, 1–18.
- Wiberg, P. L., and C. K. Harris (1994), Ripple geometry in wave-dominated environments, *J. Geophys. Res.*, *99*, 775–789.
- Williams, J. J., P. S. Bell, P. D. Thorne, N. Metje, and L. E. Coates (2004), Measurement and prediction of wave-generated suborbital ripples, *J. Geophys. Res.*, *109*, C02004, doi:10.1029/2003JC001882.
- Williams, J. J., P. S. Bell, and P. D. Thorne (2005), Unifying large and small wave-generated ripples, *J. Geophys. Res.*, *110*, C02008, doi:10.1029/2004JC002513.

M. J. Austin, T. J. O'Hare, and P. E. Russell, School of Earth, Ocean and Environmental Sciences, University of Plymouth, Drake Circus, Plymouth PL4 8AA, UK. (martin.austin@plymouth.ac.uk; tohare@plymouth.ac.uk; p.russell@plymouth.ac.uk)

G. Masselink, School of Geography, University of Plymouth, Drake Circus, Plymouth PL4 8AA, UK. (g.masselink@plymouth.ac.uk)